Influence of Polarizability on the Prediction of the Electrical Double Layer Structure in a Clay Mesopore: A Molecular Dynamics Study

Sébastien Le Crom, Christophe Tournassat, Jean-Charles Robinet, Virginie Marry

▶ **To cite this version:**

Sébastien Le Crom, Christophe Tournassat, Jean-Charles Robinet, Virginie Marry. Influence of Polarizability on the Prediction of the Electrical Double Layer Structure in a Clay Mesopore: A Molecular Dynamics Study. Journal of Physical Chemistry C, 2020, 124 (11), pp.6221-6232. 10.1021/acs.jpcc.0c00190 . hal-02875380

HAL Id: hal-02875380

https://hal.sorbonne-universite.fr/hal-02875380v1

Submitted on 19 Jun 2020

HAL is a multi-disciplinary open access archive for the deposit and dissemination of scientific research documents, whether they are published or not. The documents may come from teaching and research institutions in France or abroad, or from public or private research centers.

L'archive ouverte pluridisciplinaire **HAL**, est destinée au dépôt et à la diffusion de documents scientifiques de niveau recherche, publiés ou non, émanant des établissements d'enseignement et de recherche français ou étrangers, des laboratoires publics ou privés.

Influence of Polarizability on the Prediction of the Electrical Double Layer Structure in a Clay Mesopore: A Molecular Dynamics Study

Sébastien Le Crom,[*,†,‡] Christophe Tournassat,[¶,§,‖] Jean-Charles Robinet,[‡] and Virginie Marry[*,⊥]

†*Sorbonne Université, CNRS, PHysico-chimie des Électrolytes et Nano-systèmes InterfaciauX, PHENIX, 4 place Jussieu, F-75005, Paris, France*
‡*Agence Nationale pour la Gestion des Déchets Radioactifs (ANDRA), Parc de la Croix Blanche rue Jean Monnet, F-92298, Chatenay Malabry, France*
¶*Bureau de recherches géologiques et minières (BRGM), 3 Avenue Claude Guillemin, F-45100 Orléans, France*
§*UMR 7327 Institut des Sciences de la Terre d'Orléans, Université d'Orléans-CNRS/INSU-BRGM, F-45071 Orléans, France*
‖*Earth and Environmental Sciences Area, Energy Geosciences Division, Lawrence Berkeley National Laboratory, Berkeley, CA 94720, USA*
⊥*Sorbonne Université, UPMC Univ Paris 06, UMR 8234, PHENIX, 4 place Jussieu, F-75005, Paris, France*

E-mail: lecrom.sebastien@gmail.com; virginie.marry@sorbonne-universite.fr

Abstract

The prediction of the water and ion density profiles in the electrical double layer (EDL) is a key insight for macroscopic models that intend to model transport and swelling properties in clay materials. Unfortunately, the structure of the EDL, and especially the ion distribution, cannot be probed directly by measurements, because EDL features are inherently disturbed by direct measurement techniques. In recent years, Molecular Dynamics have provided a growing set of information on the properties of the EDL, including the properties of the diffuse layer, located beyond the Stern or compact layer, and in which a diffuse cloud of ions screens the remaining uncompensated surface charge. Molecular Dynamics results are, however, dependent on the force field used to run the simulations. In this study, we investigated the influence of the choice of a force field on the structural and dynamic properties of the EDL present at montmorillonite surface/water interfaces in a 50 Å wide slit-shaped mesopore. Simulations were run in the presence and in the absence of added NaCl, and the results were compared to ion distributions in the diffuse layer predicted with a Poisson-Boltzmann model. The simulations evidenced the strong influence of the consideration of polarizability of ions and water molecules on the predicted structural and dynamic properties of the EDL. While non polarizable force fields gave results in good agreement with the prediction of the Poisson-Boltzmann theory, our tested polarizable force field, PIM, showed very significant deviations, which could be mainly attributed to the enhanced formation of ion pairs.

Introduction

Clays have important roles in geological systems of relevance to the extraction of energy resources and the storage of energy byproducts. Clay-rich geological formations are considered as potential host rocks for radioactive waste repositories and caprocks for the long-term sequestration of CO_2. Clay-rocks also play an important role in the extraction of hydrocarbons that are increasingly accessible by hydraulic stimulation methods.[1] Clay mineral particles, the main constituent of clay-rich rocks, are constituted of stacks of layers, in which isomorphic substitutions of one cation for another of lesser charge (e.g. Mg^{2+} for Al^{3+}) is responsible for the presence of a structural negative charge. In porous clay-rich media, this negative charge is compensated next to the surfaces bordering the pores by layers of interfacial water and electrolyte ions that screen the surface charge. This region is the so-called electrical double layer (EDL), where the concentration of ions depend on the distance from the surface considered.[2] The EDL is often conceptually subdivided into two regions: the Stern layer located within the first water monolayers of the interface in which ions adsorb as inner- and outer-sphere surface complexes (ISSC, OSSC) and a diffuse layer (DL) located beyond the Stern layer in which a diffuse swarm of ions screens the remaining uncompensated surface charge.[3–8] Further away from the charged surface, the solution is neutral and is commonly described as bulk or free solution (or water). If the pore size in clay media is small enough, then the diffuse layers at adjacent surfaces bordering the pores overlap and the absence of bulk electroneutral solution in the center of the pore gives rise to a remarkable array of coupled macro-scale properties, such as swelling and semi-permeable membrane properties.[9] These coupled processes explain in large part why the mechanical, chemical, thermal osmosis and fluid transport processes in clay-rich media remain so challenging to understand and to model at all scales, from microscopic to macroscopic. Numerical methods for modeling macroscopic properties of clay media with the consideration of the presence of a EDL have met a growing interest in diverse communities in the past years. The study of EDL in porous media reaches also the community interested in the development of supercapacitors. These energy-storage devices employ EDL capacitance over a large specific area; previous works have shown that the energy density of supercapacitors can be highly increased by using nano-structured microporous electrodes.[10–13] In these perspectives, the consideration of an accurate representation of the EDL structure and dynamics is of paramount importance. The water and ion distribution and dynamics in the EDL, and especially in the DL, cannot be probed directly by measurements, because EDL features are inherently disturbed by direct measurement techniques.[14] Consequently, our knowledge of the structuration of the EDL is mainly grounded in the results of Molecular Dynamics (MD) studies. Yet, MD results are dependent on the force field used to run the simulations. MD simulations of clay-water-ion systems are currently run overwhelmingly using ClayFF,[15] a non-polarizable force field that has shown great suitability to reproduce many clay structure and water and ion dynamics experimental results.[15–40] In this force field, the short-range repulsion and dispersion are described by a Lennard-Jones potential and the electrostatic interactions by a coulombic potential between partial charges carried by the atoms. However, recent studies showed that the consideration of polarizability can have a strong influence on the outcome of simulations of mineral-water interfaces, especially in the presence of large ions.[41–46] The consideration of polarizability at montmorillonite surface/water interfaces improved also significantly the quantitative agreement of MD predictions of interlayer space structure with XRD experimental results.[47–51] However, this improvement was obtained at a significant numerical cost, and the necessity to include polarizability in clay/water MD simulations must be then evaluated as a function of the system properties of interest. In this study, we evaluated the influence of four different combinations of polarizable and non-polarizable force fields on the prediction of the structure and dynamics of water and

ions in a mesopore (width 50 Å) containing a NaCl aqueous solutions and bordered with Na-montmorillonite surfaces. The differences in MD results were then discussed in comparison with EDL continuum model descriptions that are commonly used in macroscale models.

Methods

Montmorillonite layer

Montmorillonites are 2:1 phyllosilicates in which the layers are made of an octahedral aluminum oxide sheet sandwiched between two tetrahedral silicon oxide sheets. Some Al^{3+} in the octahedral sheet are subsituted with Mg^{2+} leading to the presence of a negative structural of the layer which is compensated by counter ions in the vicinity of the surface. Montmorillonite layers have usually a *cis-vacant* structure,[52] but most of the Molecular Dynamics studies available in the the literature have been carried out using a *trans-vacant* structure. Consequently, we chose to build the structure of the montmorillonite on the basis of the *trans-vacant* structure of Brindley and Brown,[53] in order to make easier the comparisons of our results with existing data. Mg^{2+}/Al^{3+} substitutions (0.75 per unit cell) were randomly generated following an exclusion rule that prevented two magnesium atoms to occupy two neighboring octahedral sites. The surface charge was compensated by Na^+ ions. The unit cell formula was $Na_{0.75}(Al_{3.25}Mg_{0.75})Si_8O_{20}(OH)_4$.

Molecular Dynamics Force Fields

Three different force fields were used to simulate the montmorillonite layer: the original version of ClayFF,[15] a variant of ClayFF proposed by Ferrage et al., hereafter named ClayFF MOD,[54] and a polarizable force field, PIM (Polarisable Ion Model).[47] ClayFF MOD made it possible to improve the prediction of experimental neutrons and X-ray diffraction data on saponites compared to ClayFF. The main changes in this force field deal with the Van der Waals interactions between the clay surface oxygen atoms and the atoms of the fluid, for which the Lennard-Jones sigma parameter of the surface oxygen atoms is increased by 7 % compared to the original ClayFF force field. PIM was developed initially for the modeling of aqueous electrolytes,[47] and was extended more recently to include the parameters necessary to model various clay minerals and zeolites.[48–51] In this force field each atom is treated as a polarizable charged ball.

The ClayFF force field parameters have been developed in combination with the flexible SPC water model developed by Teleman et al.[55] However, many simulations of hydrated clays in the literature have been carried out using ClayFF in combination with the extended SPC force field model (SPC/E) developed by Berendsen et al.[56,57] The SPC/E force field has shown good agreement with experimental data whether at the structural or dynamic level.[58,59] In this study, ClayFF was combined either with the flexible SPC or the SPC/E water models. ClayFF MOD was combined with the SPC/E water model only. For the simulations using ClayFF and ClayFF MOD, aqueous ion parameters were obtained from Smith et al.[60] Simulations using PIM were combined with the Dang-Chang four sites water model.[61] The Dang Chang water model uses point dipoles to treat the polarizability of water molecules, similarly to PIM for clay atoms and ions. Although the Dang Chang water model was developed specifically to model liquid-gas interfaces, it reproduces well the strong polarization of water by divalent ions[62,63] and gives accurate description thermodynamic and dynamic properties of of saline solutions.[47,64]

Simulations using non-polarizable force fields were run with the LAMMPS Molecular Dynamics package[65] while simulations using PIM were run with CP2K.[66] Periodic boundary conditions were used in all directions. The cutoff radius for short-range electrostatic and repulsion-dispersion interactions was set to 10 Å. The long-range electrostatic interactions were computed using the Particle-Particle-Particle-Mesh solver[67] with a precision of 10^{-4} for the non polarizable simulations, or using the Ewald method[68] with an accuracy of 10^{-6} for polarizable simulations.

Geometry

The simulation boxes were identical for all the tested force fields, and contained 4×4 montmorillonite layer units (20.72 x 35.88 Å^2). The layer was divided in two halves placed at each vertical extremities of the box (Fig. 1). A total of 1122 water molecules were added to the pore, together with 12 sodium cations that compensated the layer charge. In the systems with added salt, two pairs of NaCl atoms were added to the pore in order to reach an average Cl^- concentration of 0.1 mol·L^{-1} in the volume of the mesopore. The vertical dimension of the box was first equilibrated in the $NPzT$ ensemble with the ClayFF force field associated with the SPC/E water model. Then, for each force field, the vertical dimensions of the boxes were slightly adjusted to retrieve the experimental densities of bulk water or of a 0.1 mol·L^{-1} NaCl aqueous solution in the center of the pore.[69] Vertical dimensions ranged from 54 Å to 55 Å depending on the system considered and the force field used in the simulation. The SHAKE algorithm[70] kept the water molecules rigid for the simulations carried out with SPC/E or Dang-Chang water models.

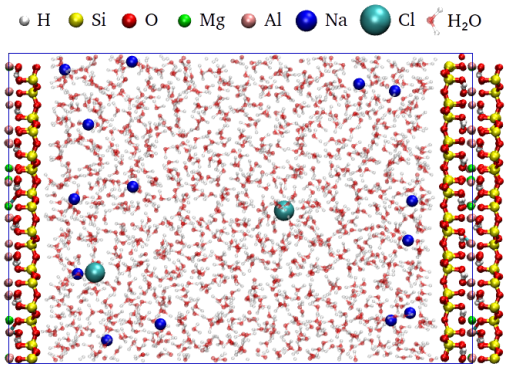

Figure 1: Snapshot of a mesopore bordered by two montmorillonite layer surfaces in the presence of 0.1 mol·L^{-1} of added NaCl. The blue frame outlines the simulation unit box that is periodically repeated in the x, y and z directions. The half-layer of montmorillonite on the right of the figure helps visualizing the periodic conditions. Atom types are shown at the top of the snapshot.

Simulation time and data post-processing

Systems run with ClayFF and ClayFF MOD were equilibrated for 20 ns in the NVT canonical ensemble at T = 300 K using a Nosé-Hoover thermostat with a time constant of 1 ps. For numerical cost reasons, systems run with PIM were equilibrated for 1 ns starting from configurations obtained from previous ClayFF-SPC/E runs. In the absence of added NaCl, the total simulation time of the production runs was set at 200 ns and 20 ns with the non-polarizable and polarizable force fields respectively. In the presence of added NaCl these values were increased to 300 ns and 80 ns respectively in order to improve the statistics of Cl^- density distribution in the pore. Density distributions perpendicular (profiles) and parallel (maps) to the montmorillonite surface were calculated on the whole trajectories. Diffusion coefficients were calculated on subsets of trajectories (20 ns and 5 ns for the non-polarizable and polarizable force fields respectively), which allowed to calculate a standard error. The diffusion coefficients parallel to the basal surfaces (xy plane), $D_{||}$, were calculated as a function of the distance to the surface with the methodology available in Liu et al.[71] and Marry et al.[5] Thus, they were evaluated from Mean Square Displacements and the survival probability chosen is the uninterrupted residence in the layer. That is, a molecule leaving at time t_1 the residence layer it had at t_0 will not be counted anymore in the calculation of the Mean Square Displacements at time $t \geq t_1$. Hydrodynamic effects result in the computation of different diffusion coefficients for equivalent bulk systems with different simulation box sizes because of the periodic boundary conditions.[64] Simonnin et al.[72] proposed an equation to correct the computed value of the diffusion coefficients for confined systems simulated in an orthorhombic box with a square base dimension L and with a pore width H. Since the simulation boxes we used do not have a square base, we do not applied correction to the diffusion coefficients in this paper. However, for informational purposes, we calculated the correction consid-

ering the average length of the base sides of our simulations, *i.e.* 28.30 Å. Taking into account the viscosity values of SPC/E,[64] Dang Chang,[64] and flexible SPC[73] water models, we obtained correction values of -1.8 $\times 10^{-10}$ $m^2 \cdot s^{-1}$, -1.63 $\times 10^{-10}$ $m^2 \cdot s^{-1}$, and -2.5 $\times$ 10^{-10} $m^2 \cdot s^{-1}$ for these three force fields respectively. It can thus be supposed that the corrections of the hydrodynamic effects in the pores modeled in this study are of the order of magnitude of these latter values.

Results and discussion

Water structure in the mesopore

The main difference in the water density profiles obtained with the tested force fields consisted in the transformation of a single high density peak in simulations run with ClayFF and ClayFF MOD into a doublet of sub-peaks in the simulations run with PIM (Fig. 2). The computation of water density profiles along the direction normal to the surface showed little to no influence of the addition of NaCl, whatever the force field used (Fig. 1 in supplementary informations).

Probability density maps of water oxygen atoms computed in the direction parallel to the surface and located at $z < 7.2$ Å were averaged over a 5×9 $Å^2$ layer unit of the clay surface (Fig. 3). In the case of PIM, high density areas, which correspond to water oxygen atoms in the first subpeak, *i.e.* closest to the surface, were observed above the center of the ditrigonal surface cavities, and the oxygen atoms belonging to the second sub peak, *i.e.* furthest from the surface, were located above the surface silicon and oxygen atoms (Fig. 3c). In the case of ClayFF and ClayFF MOD, the water oxygen atoms had only a slightly higher probability of presence above the center of the hexagonal surface cavities (Fig. 3a and Fig. 3b; note that the surface cavities had a ditrigonal shape with the PIM force field, and an hexagonal shape with the ClayFF and ClayFF MOD force fields). Radial distribution functions ($g(r)$) of ions around the water oxygen atoms present in the two sub-

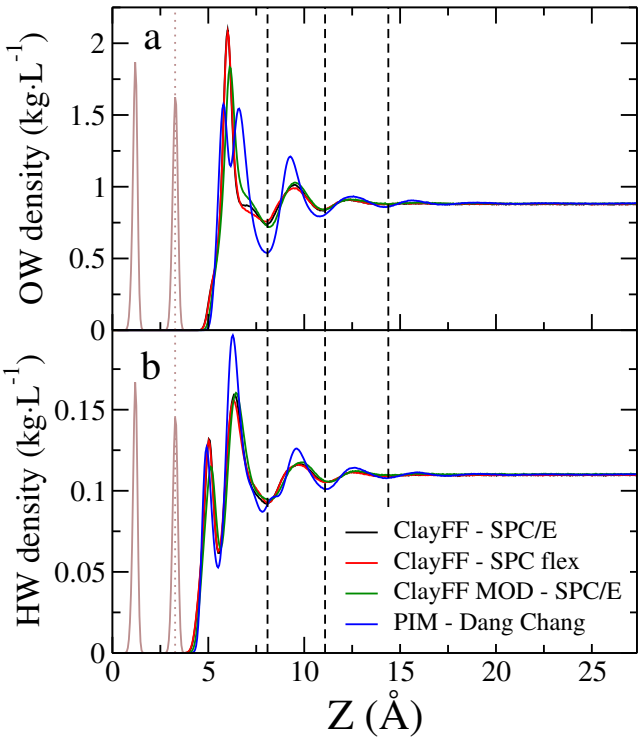

Figure 2: Density distribution profiles in the direction normal to the clay surface of (a) water oxygen atoms and (b) water hydrogen atoms. The coordinate z = 0 Å corresponds to the center of the clay layer. The clay oxygen distributions are shown in brown and the center of mass of the surface oxygen is represented by a brown dotted line at $z = 3.27$ Å. The surface water layers are delimited by the dashed black lines.

peaks revealed that the number of Na^+ in the first coordination sphere of water oxygen was equal to 0.048 Na^+ in the first subpeak, and was equal to 0.098 Na^+ in the second subpeak. Water molecules in the second subpeak were thus more involved in the hydration of sodium ions than the water molecules in the first subpeak, which interacted thus preferentially with the clay surface. The presence of two sub-peaks in the first hydration layer of the surface was not reported in the study of Tesson et al.,[50] which investigated with PIM a bi-hydrated montmorillonite interlayer space, *i.e.* a pore with a width of about 6 Å, much smaller than the pore width investigated in the present study. Because the cations that compensate the surface charge are distributed on a larger volume in a mesopore than in a bihy-

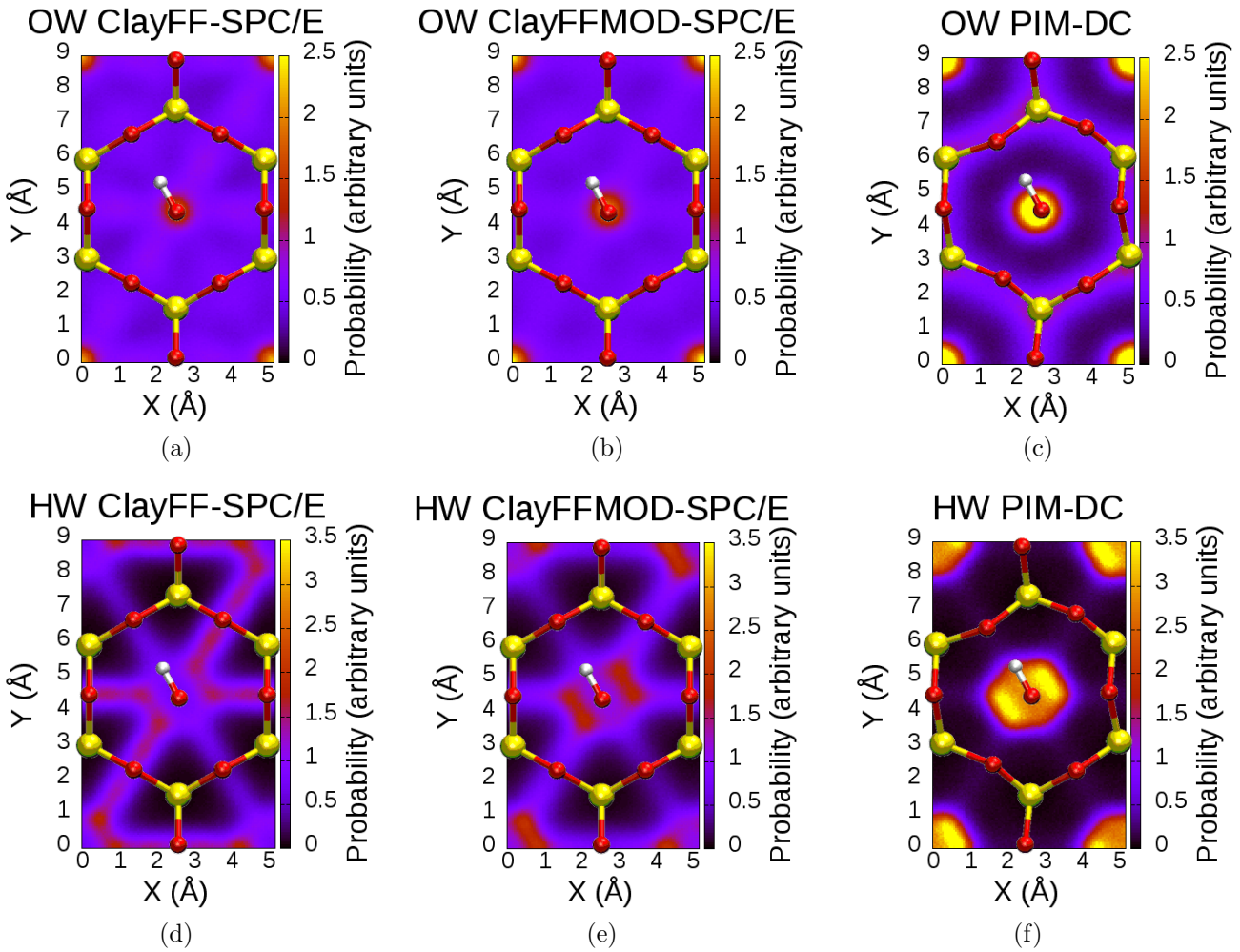

Figure 3: Atomic density maps averaged over a unit cell of the clay surface for water oxygen (a,b,c) and hydrogen (d,e,f) atoms belonging to the first hydration peak. Si (yellow), O (red) and H (white) clay atoms were drawn to show the position of the surface hexagonal (ClayFF and ClayFF MOD) or ditrigonal (PIM) cavities.

drated interlayer, in which a diffuse layer cannot form, a smaller amount of water molecules are needed to hydrate the cations close to the surface in a mesopore compared to a bihydrated interlayer. Consequently, more water molecules are free to interact with the surface, leading to the appearance of the first subpeak. All simulations predicted the existence of three ordered water layers located at very similar z values: 6.15 (considering the minimum between the two subpeaks as the center of the first peak), 9.3 and 12.5 Å for the PIM simulation, 6.15 Å , 9.55 Å and 12.4 Å for the simulations with ClayFF MOD, and 6.0 Å , 9.5 Å and 12.4 Å for the simulations with ClayFF. The spacing between the oxygen water density peaks was close to the diameter of a water molecule, indicating that the water layering was mainly due to steric packing at the clay mineral-water interface. The type of water model had very little influence on the structure of the water molecules at the interface. Indeed, the distributions of water oxygen and hydrogen atoms were almost similar, the only difference being a more pronounced shoulder at 7.3 Å for the simulation run with the SPC/E model compared to the SPC model. The last remarkable feature about the water distributions was the slight repulsion (about 0.15 Å) of water molecules from the surface for the systems simulated with ClayFF MOD compared to ClayFF. This result was in agreement with the increased size of the sur-

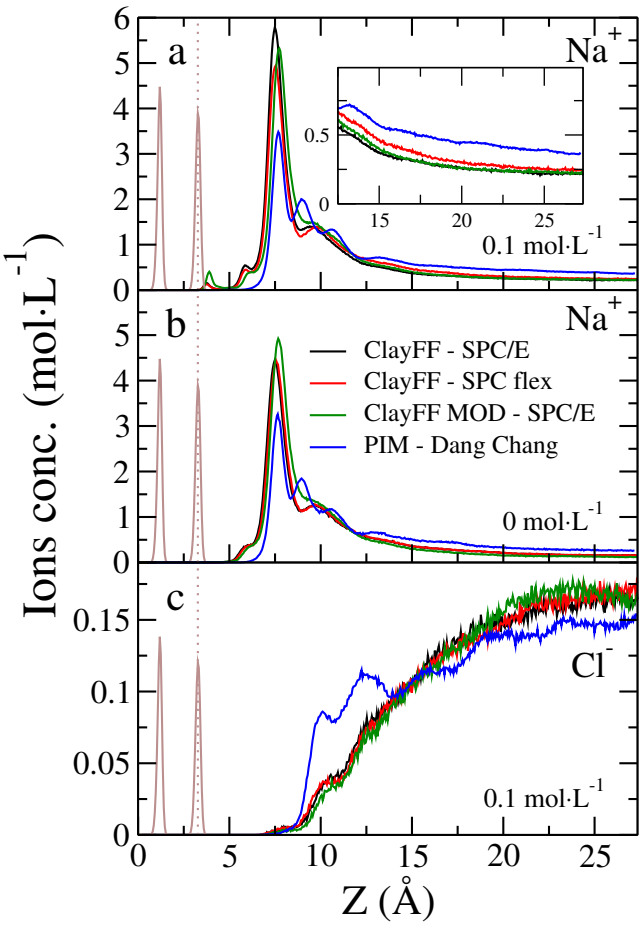

Figure 4: Na^+ and Cl^- density distribution profiles in the direction normal to the clay surface. (a) Na^+ density profile in the presence of added 0.1 mol·L^{-1} NaCl. (b) Na^+ density profile in the absence of added NaCl. (c) Cl^- density profile in the presence of added 0.1 mol·L^{-1} NaCl. The coordinate z = 0 Å corresponds to the center of the clay layer. The density distributions of clay oxygen atoms are shown in brown and the center of mass of the surface oxygen atoms is represented by a brown dotted line at z = 3.27 Å. The inset in figure (a) focuses on the region located between 12.5 Å and 27.4 Å and helps to visualize the tail in the Na^+ density distributions.

face oxygen atoms in ClayFF MOD compared to ClayFF.

The density distribution profiles of water hydrogen atoms along the axis normal to the surface were very similar for all tested force fields. The first peak was slightly closer to the surface and the density oscillations had greater amplitudes with PIM than with ClayFF and ClayFF MOD. The use of the SPC/E water model or of the flexible SPC water model did not have any influence on the results obtained with ClayFF. Probability density maps of water hydrogen atoms computed in the direction parallel to the surface showed the presence of patterns that were nearly identical for all the simulations run with non polarizable force fields (Fig. 3d and 3e). Water hydrogen atoms were located above the center of the cavities or above the surface oxygen atoms, which they formed hydrogen bonds with. In the case of the polarizable force field, the water hydrogen density was the largest above the center of the cavities (Fig. 3f). These observations confirmed that water molecules close to the clay surfaces were more structured with PIM than with the tested non polarizable force fields. At last, all density maps evidenced the low probability for water to form hydrogen bonds with the surface oxygen atoms along the direction parallel to that of the clay hydroxyl groups (Fig. 3d, 3e and 3f).

Aqueous ion distributions

The addition of NaCl in the system had little influence on the Na^+ distribution profiles in the region closest to the surface. The sodium density peaks remained at the same position and the slight differences in intensity could be attributed to the highest overall concentration of sodium in the system in the presence of added NaCl (Fig. 4). The comparison of the results obtained with the tested force fields revealed a significant influence of the consideration of the polarizability on the profiles. First, a small Na^+ density peak was observed at a very short distance from the surface (about 0.5 Å) when non polarizable force fields were used (Fig. 4a). This peak can be attributed to the presence of Na^+ adsorbed in inner-sphere complexes, which partially dehydrate to coordinate with the surface. The first hydration sphere of these cations contained only 3.1 water molecules, to be compared to 5.8 water molecules in the bulk. These cations entered partially the surface hexagonal cavities that were the closest to clusters of oc-

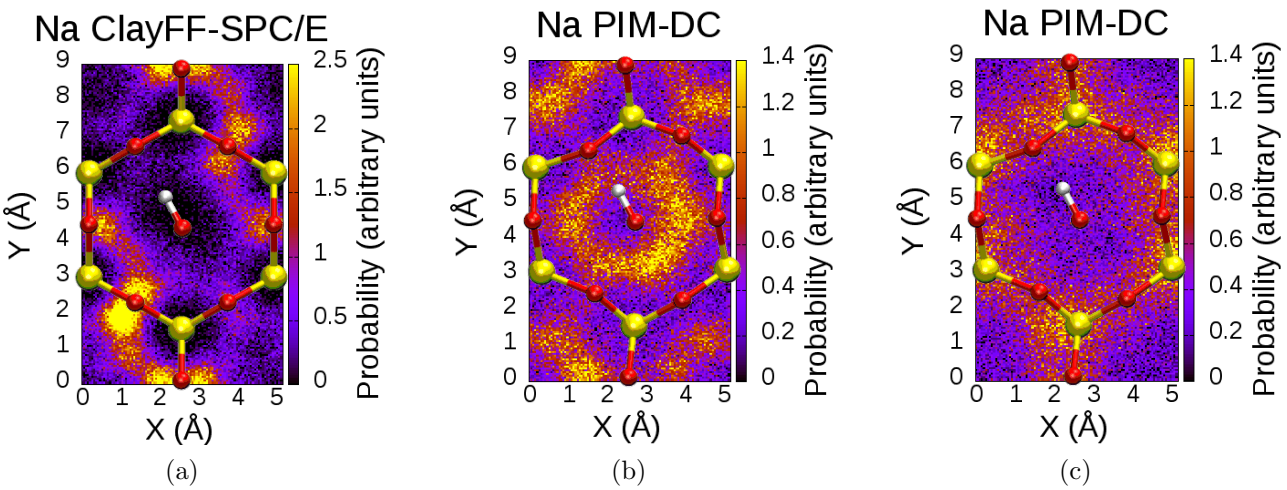

Figure 5: Atomic density maps averaged over a unit cell of the clay surface of (a) inner-sphere sodium ions (ClayFF) (b) sodium ions in the the first peak (PIM) and (c) sodium ions in the the second peak (PIM). Si (yellow), O (red) and H (white) clay atoms were drawn to show the position of the surface hexagonal (ClayFF and ClayFF MOD) or ditrigonal (PIM) cavities.

tahedral substitutions, therefore in surface regions where the negative charge of the clay was the highest in amplitude. These inner-sphere adsorbed cations were not observed with the PIM force field because of the deformation of the surface cavities from an hexagonal to a ditrigonal shape, which prevented cations from entering the cavities.[49,50] The hexagonal cavities obtained with the non-polarizable forcefields had conversely a center position that was accessible to small cations such as sodium. The Na^+ density distribution profiles obtained with non polarizable force fields exhibited also a shoulder at 5.9 Å, which also corresponds to inner-sphere adsorbed sodium but with a higher hydration number (4.4). The density map evidenced a preferential position of cations belonging to this peak above the surface oxygen atoms (Fig. 5a).

The first peak of Na^+ adsorbed in outer-sphere complexes was located at a distance to the surface that was similar for all tested force fields. The density maps of these first outer-sphere cations exhibited a similar pattern, with preferential sodium positions (see Fig. 5b for PIM ; other force fields gave similar distribution patterns). Differences in peak intensity were significant. The curves produced from the simulations using ClayFF with SPC and SPC/E overlapped almost perfectly, while the simulation done with ClayFF MOD and SPC/E resulted in a slight shift of the peak position and a difference in intensity. These differences evidenced the influence of the clay force field on the structure of the peak of cations adsorbed in outer-sphere complexes. Further away from the surface, the differences between the force fields were more significant. The sodium density distributions obtained with ClayFF and ClayFF MOD exhibited a shoulder or a very small peak at 9.6 Å, whereas the sodium density distribution obtained with PIM exhibited a second and a third distinct peak at 9 Å and at 10.7 Å respectively. Polarization may thus play an important role in the structuring of cations at distances from the surface beyond the first adsorption peak. Sodium ions in this second and third peak were not homogeneously distributed in the direction parallel to the surface (Fig. 5c). The most probable density areas of the cations in the first adsorption peak were the least likely areas in the second peak, and conversely. This 3D organization of Na^+ next to the surface minimized repulsive electrostatic interactions. The density distribution of cations simulated with non polarizable force fields did not present any specific 3D organization beyond the first outer-sphere adsorption peak. Because of this

difference of ion structuration next to the surface, the sodium concentrations predicted in the center part of the pore were also different with polarizable and non-polarizable force fields: 0.35 mol·L^{-1} with PIM, *i.e.*, 0.24 mol·L^{-1} with ClayFF/flexible SPC, and 0.22 mol·L^{-1} with ClayFF /rigid SPC/E. The Na^+ concentration profiles produced with the ClayFF and ClayFF MOD force fields in combination with the SPC/E model started to overlap with increasing distance from the surface and reached the same concentration in the center of the pore, whereas the Na^+ concentration profile produced with ClayFF and the flexible SPC model was slightly higher. Consequently, the structure of adsorbed cations was governed by different interactions depending on the distance to the surface. The structuration of the inner-sphere adsorption peak was mainly controlled by the clay force field, while the structuration of the adsorbed cations beyond this first peak was dictated by the water model up to the center of the pore. Previous studies have shown that the consideration of polarizability can dramatically change the predictions of ion distributions of ions at air/water interfaces.[41–44] The present study showed that a similar effect could be observed for a clay mineral/water interface.

In the presence of added NaCl, Cl^- anions were repelled from the negatively charged montmorillonite surface, in agreement with previous MD investigations results.[5–7,27,72,74–76] The distance of closest approach to the surface was 6.8 Å for ClayFF, 7 Å for ClayFF MOD and 7.1 Å for PIM, where the position $z = 0$ refers to the center of the clay layer (Fig. 4c). The distributions of anions simulated with the non-polarizable force fields had a density shoulder around 10.3 Å , which corresponded to the end of the outer-sphere sodium density peak. The concentration in the center of the pore was 0.16 mol·L^{-1} and 0.17 mol·L^{-1} with the SPC/E and flexible SPC force fields respectively. These anion concentrations were lower than the cation concentrations, thus evidencing the overlap of the diffuse layers in the investigated conditions. The distribution of chloride ions obtained with PIM exhibited density peaks

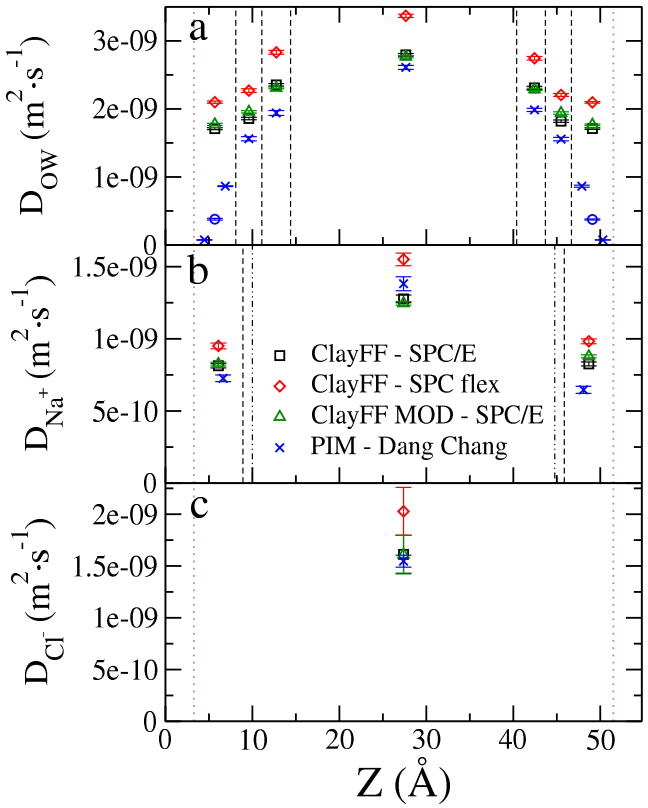

Figure 6: $D_{||}$ of (a) water oxygen, (b) sodium ions and (c) chloride ions. The two brown dotted lines at z = 3.27 Å and z = 51.5 Å correspond to the averaged position of surface oxygen atoms. The dashed black lines (black dashed-dot-dot vertical lines for Na^+ in the case of simulations run with PIM) indicate the different layers in which Na^+ and H_2O diffusion coefficients were calculated. Chloride diffusion coefficients were calculated on the whole pore. The cross symbols in the layers closest to the surface correspond to $D_{||}$ values of water molecules in each of the two density subpeaks observed in PIM simulations. The circle symbol corresponds to the $D_{||}$ value calculated in the whole first water layer (2 subpeaks). The exact values of the layers z coordinates are given in the Tab. 1 and Tab. 2 together with the diffusion coefficients.

or oscillations at 10 Å , and 12.5 Å . Even if the statistics was of lesser quality for anion than for cation distribution (there were only two Cl^- in the box), it remained clear that the concentration of anions increased more abruptly with the distance to the surface in the simulations using PIM than in those using the

non-polarizable force fields. Thus, the long-range structuring of cations observed with PIM was also observed with the anions. The radial distribution functions of Na^+ ions around the Cl^- ions located at $z < 14$ Å indicated that more Na^+-Cl^- ion pairs were formed in simulation run with PIM compared to the other force fields: 0.12 sodium for ClayFF/SPC flex, 0.11 sodium for ClayFF/SPC/E and 0.08 for ClayFF MOD/SPC/E, versus 0.44 Na^+ for PIM. The increased formation of ion pairs with PIM was thus responsible for the appearance of Cl^- density peaks next to the outer-sphere Na^+ density peaks. Previous studies have shown that the osmotic coefficients obtained in electrolyte solutions with common non polarizable force fields were too large.[77] A possible explanation would be that ions in solution did not form enough pairs in Molecular Dynamics because of bad potentials to describe the ion-ion interactions. Indeed, in traditional force fields only the ion-water potentials are fitted in order to obtain the good single-ion properties in water, the ion-ion parameters are then obtained by simple mixing rules which may be inadequate to provide a suitable description of concentrated aqueous solutions. A further study would be necessary to know if the addition of the polarizability is necessary or if only a better fit of ion-ion potentials would be enough. in any case, it seems that the PIM force field allows to form more ion pairs in solution, that is a step in the right direction.

Diffusion in the mesopore

$D_{||}$ values were calculated for H_2O in the three water layers stacked on the surface represented by the three peaks near the clay/fluid interface of the OW distributions (Fig. 2a), as well as in the center of the pore. We also calculated the $D_{||}$ values for Na^+ in the first peak of the vertical distribution and in the center of the pore (Fig. 6, Tab. 1 and Tab. 2). The $D_{||}$ values obtained for H_2O depended on the considered force fields: 2.61 $\times 10^{-9}$ $m^2 \cdot s^{-1}$ for PIM, 2.79 $\times 10^{-9}$ $m^2 \cdot s^{-1}$ for SPC/E and 3.37 $\times 10^{-9}$ $m^2 \cdot s^{-1}$ for SPC flex. All these values were larger than the experimental value for bulk water (2.3 $\times$ 10^{-9} $m^2 \cdot s^{-1}$).[78] The value obtained with for SPC flex was however smaller than the value reported in the original study[55] (6.1 $\times$ 10^{-9} $m^2 \cdot s^{-1}$) because the system was not equilibrated in this study. However, it is in much better agreement with the value of 3.6 $\times$ 10^{-9} $m^2 \cdot s^{-1}$ reported in the Wallqvist et al.[79] study and it is also consistent with the value reported by Greathouse et al.[18] (3.28 $\times$ 10^{-9} $m^2 \cdot s^{-1}$) for a bulk water system with a low concentration of NaCl similar to the one used in our study. An independent calculation of the H_2O diffusion coefficient in a box containing only SPC flex water molecules without added salt nor clay resulted in a value of 3.33 $\times 10^{-9}$ $m^2 \cdot s^{-1}$, consistent with the coefficient values calculated in the center of the pore in the presence of clay surfaces and added NaCl.

$D_{||}$ values obtained for H_2O in the different water layers were very similar with ClayFF - SPC/E and ClayFF MOD - SPC/E. Simulation run with ClayFF-MOD resulted in a slightly higher water mobility in the two layers close to the surface compared to simulations run with ClayFF. This difference can be explained by the larger repulsion of water molecules from the surface with this force field compared to the original ClayFF force field. With ClayFF and ClayFF MOD force fields, $D_{||}$ values increased monotonically from the surface to the bulk water, with little difference (less than 10 %) between the first and the second surface layer of water. In previous studies, a smaller $D_{||}$ value was found in the second surface layer compared to the first layer,[5,80] but the atoms of the clay structure were kept fixed during these simulations in these studies, which may have influenced the diffusion of the species in the neighboring pore.[24] Greathouse et al.[18] simulated a sodium montmorillonite mesopore using ClayFF, SPC flex and Smith and Dang force field. The increase in water diffusion coefficient between the first layer and second layer was found to be equivalent to that between the second layer and third layer. The difference in results with our study may be related to a difference of montmorillonite layer charge (1 charge per unit cell in Greathouse et al. study versus

Table 1: $D_{||}$ of water following the force field used. The coefficients given as well as the errors are an averages of the values obtained in two symmetric layers. The value taken for D_0 is the value calculated at the center of the pore, assimilated to bulk. For PIM are given the coefficient calculated in the whole first layer as well as those obtained in the two subpeaks.

OW	1^{st} layer	2^{nd} layer	3^{rd} layer	bulk
ClayFF - SPC/E	(3.27 - 8.08 Å)	(8.08 - 11.08 Å)	(11.08 - 14.38 Å)	(14.38 - 27.35 Å)
D (10^{-9} $m^2 \cdot s^{-1}$)	1.71 ± 0.014	1.84 ± 0.018	2.33 ± 0.021	2.79 ± 0.019
D / D_0	0.61 ± 0.01	0.66 ± 0.01	0.83 ± 0.01	1.00 ± 0.01
ClayFF - SPC flex	(3.27 - 8.08 Å)	(8.08 - 11.08 Å)	(11.08 - 14.38 Å)	(14.38 - 27.35 Å)
D (10^{-9} $m^2 \cdot s^{-1}$)	2.10 ± 0.014	2.24 ± 0.025	2.79 ± 0.028	3.37 ± 0.025
D / D_0	0.62 ± 0.01	0.66 ± 0.01	0.83 ± 0.01	1.00 ± 0.01
ClayFFMOD - SPC/E	(3.27 - 8.18 Å)	(8.18 - 11.08 Å)	(11.08 - 14.38 Å)	(14.38 - 27.35 Å)
D (10^{-9} $m^2 \cdot s^{-1}$)	1.77 ± 0.013	1.95 ± 0.017	2.30 ± 0.014	2.76 ± 0.017
D / D_0	0.64 ± 0.01	0.7 ± 0.01	0.83 ± 0.01	1.00 ± 0.01
PIM - Dang Chang	(3.27 - 8.08 Å) (3.27 - 6.16 Å) (6.16 - 8.08 Å)	(8.08 - 10.78 Å)	(10.78 - 14.18 Å)	(14.18 - 27.35 Å)
D (10^{-9} $m^2 \cdot s^{-1}$)	0.38 ± 0.010 0.074 ± 0.003 0.86 ± 0.010	1.56 ± 0.028	1.96 ± 0.030	2.61 ± 0.030
D / D_0	0.14 ± 0.005 0.03 ± 0.001 0.33 ± 0.008	0.60 ± 0.02	0.75 ± 0.02	1.00 ± 0.02

Table 2: $D_{||}$ of ions following the force field used. The sodium coefficients given as well as the errors are an averages of the values obtained in two symmetric layers. The value taken for D_0 is the value calculated at the center of the pore, assimilated to bulk. For PIM the first sodium layer was attributed to the 2 first peaks in the distribution. The chloride diffusion coefficients were calculated on the whole pore.

Na^+	1^{st} peak	bulk	Cl^- all pore
ClayFF - SPC/E	(3.27 - 8.9 Å)	(8.9 - 27.35 Å)	(3.27 - 27.35 Å)
D (10^{-9} $m^2 \cdot s^{-1}$)	0.81 ± 0.014	1.28 ± 0.057	1.61 ± 0.018
D / D_0	0.64 ± 0.02	1.00 ± 0.04	-
ClayFF - SPC flex	(3.27 - 8.9 Å)	(8.9 - 27.35 Å)	(3.27 - 27.35 Å)
D (10^{-9} $m^2 \cdot s^{-1}$)	0.97 ± 0.018	1.55 ± 0.043	2.03 ± 0.023
D / D_0	0.62 ± 0.03	1.00 ± 0.05	-
ClayFFMOD - SPC/E	(3.27 - 9.2 Å)	(9.2 - 27.35 Å)	(3.27 - 27.35 Å)
D (10^{-9} $m^2 \cdot s^{-1}$)	0.85 ± 0.011	1.25 ± 0.013	1.61 ± 0.019
D / D_0	0.68 ± 0.02	1.00 ± 0.02	-
PIM - Dang Chang	two first peaks (3.27 - 10.0 Å) (3.27 - 8.40 Å) (8.40 - 10.0 Å)	(10.0 - 27.35 Å)	(3.27 - 27.35 Å)
D (10^{-9} $m^2 \cdot s^{-1}$)	0.69 ± 0.024 0.62 ± 0.03 0.69 ± 0.03	1.38 ± 0.048	1.55 ± 0.058
D / D_0	0.50 ± 0.04 0.44 ± 0.03 0.49 ± 0.03	1.00 ± 0.07	-

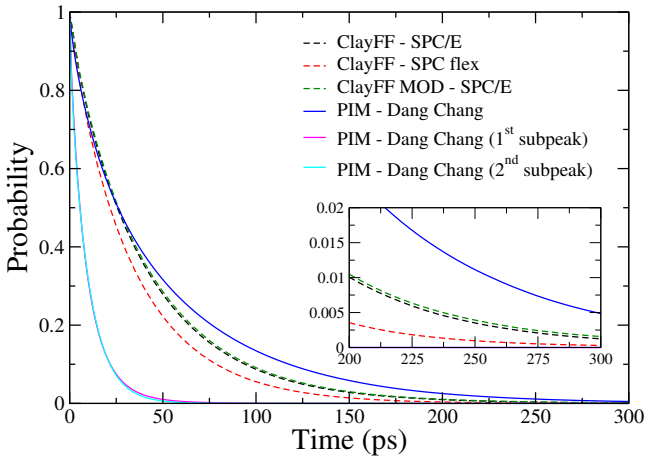

Figure 7: Survival probabilities of the water molecules in the layer the closest to the surface as a function of time. The survival probabilities of the water molecules in the two subpeaks of the polarizable water distributions were also represented in light blue and in pink. In the inset is represented a zoom of the different probabilities between 200 ps and 300 ps.

0.75 charge per unit cell in this study), because an increase of surface charge induced an increase of the electrostatic field at the interface, leading in turn to a decrease of water and ions mobility.[81]

The consideration of polarizability led to noticeable differences in results. First, in all layers, the values of the water $D_{||}$ obtained with PIM were lower than $D_{||}$ obtained with non polarizable force fields, an observation that was consistent with the lower bulk $D_{||}$ value obtained with PIM. Second, the decrease of the diffusion coefficient at the surface relative to the center of the pore was larger with PIM than with any of the non-polarizable force fields (Tab. 1). Water molecules in the subpeak the closest to the surface, which are located above the center of the surface cavities, were much less mobile than those of the second subpeak. The $D_{||}$ value calculated over the whole first peak was equivalent to the average of the coefficients in the two subpeaks.

The survival probabilities of water molecules, *i.e.* the probability of a molecule to remain in a given layer from time 0 to time t, was very low in the subpeak that was the closest to the surface. The survival probability in the second subpeak was similar, the survival probabilities in the two subpeaks overlap (Fig. 7). However, the survival probability in the whole first peak was very high compared to the survival probability in within the two sub-peaks, which indicates that a rapid exchange of molecules took place between the two subpeaks. Finally, the decrease in the survival probability of the water molecules in the first peak at short times was similar for all other force fields. In contrast with the behavior of water molecules, the diffusion coefficients of sodium, as well as of chloride were very similar with polarizable and non-polarizable force-fields.

Comparison with Poisson-Boltzmann theory

Molecular Dynamics predictions of the EDL structure have been often compared to continuum models that can be used in macroscopic predictions with applications in coupled water and ion transport processes in clay media.[6,14,27,74,76,82,83] A popular model is the so-called modified Gouy-Chapman (MGC) model that is based on the Poisson-Boltzmann equation. In this model, infinite and flat surfaces are considered to be uniformly charged with a surface charge density σ, the solvent is a continuum defined by its dielectric constant ϵ_r, and the statistical correlations between ions, which are assumed to be point-charge, are neglected (see annex). The modified Gouy-Chapmann model also considers a distance of closest approach of ions to the surface d_0. In our systems the size of the pore, the amount of added salt and the surface charge were known, leaving d_0 as the sole parameter that could be adjusted to fit the MD density profiles. Usually, the distance of closest approach is representative of the ionic radius of the species of interest. In the present study, we considered also large values that extended beyond the first density peak of water or Na^+. This hypothesis could be seen as a simplified approach to describe the presence of a Stern, or compact, layer at the surface. In practice, we considered that all ions located at a distance from the surface lower than d_0 did

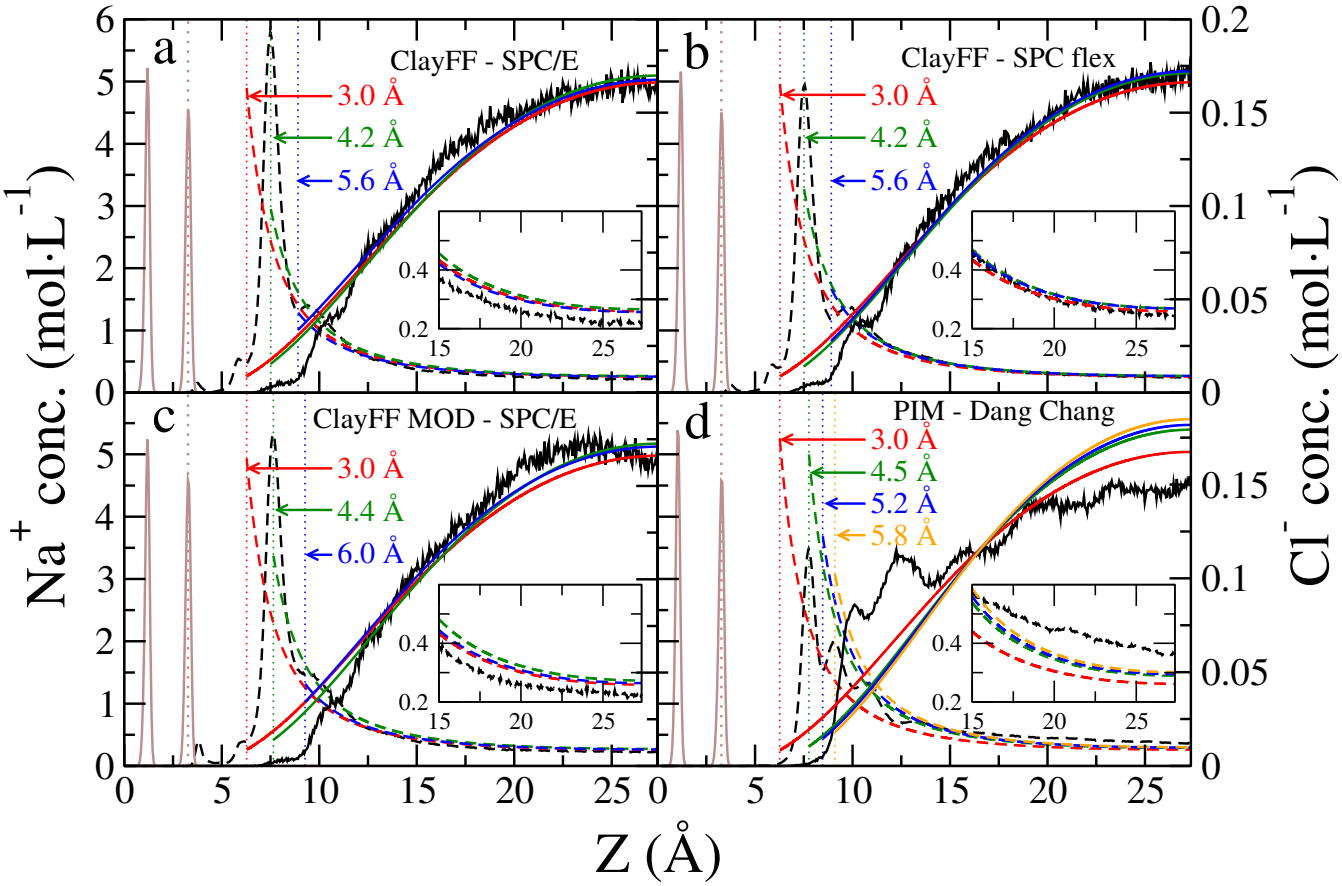

Figure 8: Ionic distributions obtained by Molecular Dynamics and the ones calculated by Poisson-Boltzmann for the different distances of closest approach defined by vertical dotted lines: (a) ClayFF-SPC/E, (b) ClayFF - SPC flex, (c) ClayFF MOD - SPC/E and (d) PIM - Dang Chang. The distributions obtained by Molecular Dynamics are represented in black, those calculated by Poisson-Boltzmann in colors corresponding to each d_0 defined on the graphs. Na^+ distributions are shown in dashed lines whereas Cl^- distributions are represented by solid lines. The left and right vertical axes refer to sodium and chloride distributions respectively. All insets are zooms of the cationic distributions between 15 Å and 27.35 Å.

not belong to the diffuse layer, *i.e.* their charge was added to the value of the surface charge σ. We tested various positions for the d_0 value that corresponded to the main features observed on the MD density distributions, *i.e.* before the first outer sphere peak of the cations, at the top of the first peak and just after the first peak. Because the distribution of sodium was much more structured with PIM than with the other force fields, we chose an additional fourth distance corresponding to the top of the second density peak of Na^+ (Fig. 8).

Regardless of the chosen distance of closest approach, the predictions of the Poisson-Boltzmann equation was in reasonable agreement with the ion density distributions obtained with the non-polarizable force fields. This result was in agreement with similar comparisons reported in the literature.[27,74] The combination of ClayFF with the SPC flex force field gave the best agreement with the Poisson-Boltzmann equation prediction, regardless of the chosen distance of closest approach. The agreement was not as good with the simulation run with PIM. This result was actually not surprising because the Poisson-Boltzmann equation cannot represent ion-ion interactions that were found to be stronger when polarization was taken into account in our MD simulations. The tails in the density profiles after the ions layer structuring at short distance from the surface had small curvatures in the case of PIM

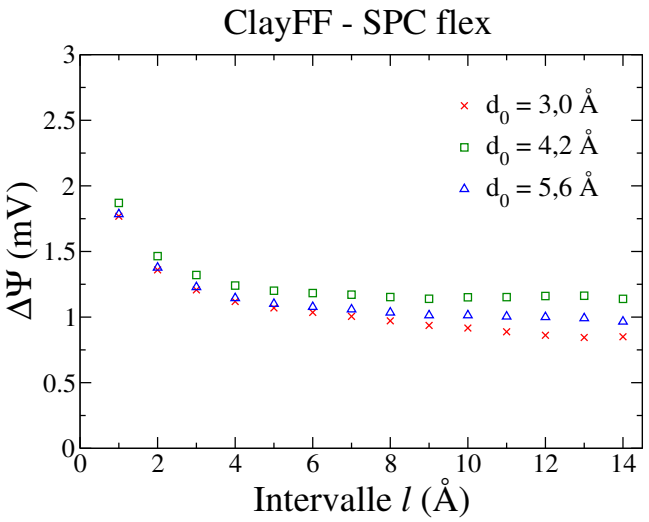

Figure 9: Potential difference average between Molecular Dynamics (ClayFF-SPC flex) and the potentials calculated by Poisson-Boltzmann for various distances of closest approach as a function of the selected interval. l corresponds to an interval of z taken symmetrical around the center of the pore. So point $l = 1.0$ corresponds to the interval [26.35; 27.35].

resulting in larger differences of concentrations at the pore center between the cations and the anions, which also did not compare well with the Poisson-Bolzmann equation long-range behavior.

We calculated the electrostatic potential as a function of the distance z from the surface, defined by:

$$\psi(z) = -\frac{RT}{2F} \ln\left(\frac{C_{Na^+}(z)}{C_{Cl^-}(z)}\right) \qquad (1)$$

with R the gas constant, F the Faraday constant, T the temperature, and C_{Na^+} and C_{Cl^-} the concentrations of cations and anions at a distance z from the surface. The average of the potential difference $\Delta\psi$ between MD and the PB distributions is then given by:

$$\Delta\Psi = \frac{1}{l}\int_{z_{max}-l}^{z_{max}} |\Psi_{PB}(z) - \Psi_{MD}(z)|\, dz \qquad (2)$$

with z_{max} the z coordinate of the center of the pore (in our case 27.35 Å) and l the interval size considered for the calculation. For the smallest l, the distance of 3.0 Å gave the best agreement with the MD density distributions obtained with non-polarizable force field (Fig. 9). Therefore the diffuse layer would begin around 3.0 Å from the surface, *i.e.* at two ionic radii of adsorbed species, which is in agreement with the modified Gouy-Chapman model assumptions. No satisfactory agreement could be obtained with the density distributions obtained with PIM.

The main motivation for the addition of a distance of closest approach d_0 is to mimic the finite size of the ions at the vicinity of the surface. Other approaches exist to take the finite size of ions into account. In particular, the modified Poisson-Boltzmann equation describes the ion distributions by Fermi distributions instead of Boltzmann distributions. The modified Poisson-Boltzmann equation has given good results in the vicinity of charged surfaces for electrolytes with large ions and for ionic liquids.[84,85] In a further study, the present MD results could help to benchmark these other approaches.

Some studies have attempted to account for polarization effects into the framework of Poisson-Boltzmann theory.[86–88] Although this is outside the scope of this study, our MD polarizable simulations would enable to benchmark these models.

Conclusion

The consideration of polarizability had a marked influence on the MD prediction of structural and dynamic properties of the diffuse layer present in mesopores bordered by clay mineral surfaces. The use of a polarizable force field led to an increase structuration of water molecule at the vicinity of the clay surfaces, which led in turn to a decrease of the mobility of water molecules compared to results obtained from simulations with non polarizable force fields. The ionic distributions showed also a stronger layering near the surfaces with a polarizable force field than with non polarizable force fields. Ion-pairing was also more intense with a polarizable force field. While the MD ion density profiles beyond the compact layer in the EDL was in good agreement with the

prediction of the Poisson-Boltzmann model in simulation run with non-polarizable force fields, this agreement broke apart in simulations run with a polarizable force field.

Because there is no direct experimental evidence of the structure or dynamics of the EDL, it is difficult to answer with certainty to the question of the force field choice. However, PIM has already shown a very good agreement with the experiments on the structure of concentrated solutions[47,89] as well as on the structure of clays.[48–51] We can thus assume that PIM may correctly describe the structure of the species at the interface. To test this assumption, it would be interesting to reproduce this study on clays more tractable experimentally, such as muscovites, on which reflectivity studies can be conducted.[4]

Finally, it seems that Poisson-Boltzmann is accurate enough to describe the structure of ions inside mesopores when one goes to higher scales such as in surface complexation, swelling or reactive transport models.[14,27,90–92] It would be interesting to see the sensitivity of these macroscopic modeling approaches to EDL descriptions following the electrical potentials given by PIM and see if the results vary significantly from the PB-based ones.

Supporting Information Available

- Density distributions profiles of water atoms in the presence and in the absense of added 0.1 mol·L^{-1} NaCl.
- LAMMPS input file for ClayFF-SPC/E force field.
- CP2K input file for PIM-Dang Chang force field.
- Topology file in xyz format.

Acknowledgement This work is part of the Ph.D. project of S.L.C., which was funded by the French National Agency for Radioactive Waste Management (Andra). The authors also acknowledge for HPC ressources granted by GENCI (TGCC and Cines, Grant No.A0040410107) and Sorbonne Université (MeSu).

Annex

The Poisson-Boltzmann equation describes the distribution of the electric potential in solution in the direction normal to a charged surface. Thanks to the Boltzmann statistic, we can express the concentration c_i of an ion i as a function of the distance r of a central particle such as:

$$c_i(r) = M_i \exp\left(-\frac{V_i(r)}{k_\mathrm{B}T}\right)$$

where $V_i(r)$ can be identified with the electrostatic energy:

$$V_i(r) = e_i\psi(r)$$

with $e_i = Z_i e$ the charge of the ion i and $\psi(r)$ the electrostatic potential.

Between two uniformly charged planes, the ionic concentration c_i and the electrostatic potential ψ depend only on the direction normal to the planes z. We thus obtain by integrating c_i between the two planes:

$$\begin{aligned}\int_{-L/2}^{+L/2} c_i(z)\mathrm{d}z &= M_i \int_{-L/2}^{+L/2} \exp\left(-\frac{e_i\psi(z)}{k_\mathrm{B}T}\right)\mathrm{d}z \\ &= Lc_i^0\end{aligned}$$

with L the distance between the two planes and c_i^0 the average concentration of the ion i inside the pore.

This equation allows to calculate M_i and by replacing $\Delta\psi = -\sum_i e_i c_i(r)/\epsilon_0\epsilon_r$ in the Poisson equation, we obtain:

$$\Delta\psi = -\sum_i \frac{e_i M_i}{\epsilon_0\epsilon_r} \exp\left(-\frac{e_i\psi}{k_\mathrm{B}T}\right)$$

The Poisson-Boltzmann equation can be solved analytically with a monovalent counterions present between the two planes. When the valence of the ions is greater than one or if ions of opposite charge are also present in the system, as in the case of the presence of saline solutions, the equation can not be solved analytically and must thus be solved numerically.[2,93,94]

References

(1) Tournassat, C.; Bourg, I. C.; Steefel, C. I.; Bergaya, F. *Natural and Engineered Clay Barriers*; Elsevier, 2015; Vol. 6.

(2) Sposito, G. *The surface chemistry of natural particles*; Oxford University Press, 2004.

(3) Lee, S. S.; Fenter, P.; Park, C.; Sturchio, N. C.; Nagy, K. L. Hydrated cation speciation at the muscovite (001)-water interface. *Langmuir* **2010**, *26*, 16647–16651.

(4) Lee, S. S.; Fenter, P.; Nagy, K. L.; Sturchio, N. C. Monovalent ion adsorption at the muscovite (001) solution interface: relationships among ion coverage and speciation, interfacial water structure, and substrate relaxation. *Langmuir* **2012**, *28*, 8637–8650.

(5) Marry, V.; Rotenberg, B.; Turq, P. Structure and dynamics of water at a clay surface from Molecular Dynamics simulation. *Phys. Chem. Chem. Phys.* **2008**, *10*, 4802–4813.

(6) Tournassat, C.; Chapron, Y.; Leroy, P.; Boulahya, F. Comparison of Molecular Dynamics simulations with triple layer and modified Gouy-Chapman models in a 0.1 M NaCl - montmorillonite system. *J. Colloid Interface Sci.* **2009**, *339*, 533–541.

(7) Rotenberg, B.; Marry, V.; Vuilleumier, R.; Malikova, N.; Simon, C.; Turq, P. Water and ions in clays: Unraveling the interlayer/micropore exchange using Molecular Dynamics. *Geochim. Cosmochim. Acta* **2007**, *71*, 5089–5101.

(8) Bourg, I. C.; Sposito, G. Molecular Dynamics simulations of the electrical double layer on smectite surfaces contacting concentrated mixed electrolyte (NaCl-CaCl2) solutions. *J. Colloid Interface Sci.* **2011**, *360*, 701–715.

(9) Tournassat, C.; Steefel, C. I. Reactive transport modeling of coupled processes in nanoporous media. *Rev. Mineral. Geochem.* **2019**, *85*, 75–110.

(10) Burt, R.; Breitsprecher, K.; Daffos, B.; Taberna, P.-L.; Simon, P.; Birkett, G.; Zhao, X.; Holm, C.; Salanne, M. Capacitance of nanoporous carbon-based supercapacitors is a trade-off between the concentration and the separability of the ions. *J. Phys. Chem. Lett.* **2016**, *7*, 40154021.

(11) Fedorov, M. V.; Kornyshev, A. A. Ionic liquids at electrified interfaces. *Chem. Rev.* **2014**, *114*, 2978–3036.

(12) Rochester, C.; Sartor, A.; Pruessner, G.; Kornyshev, A. "One dimensional" double layer. The effect of size asymmetry of cations and anions on charge-storage in ultranarrow nanopores-an Ising model theory. *Russ. J. Electrochem.* **2017**, *53*, 11651170.

(13) Bossa, G. V.; Downing, R.; Abrams, J.; Berntson, B. K.; May, S. Differential capacitance of electrolytes at weakly curved electrodes. *J. Phys. Chem. C* **2018**, *123*, 1127–1135.

(14) Bourg, I. C.; Lee, S. S.; Fenter, P.; Tournassat, C. Stern layer structure and energetics at mica-water interfaces. *J. Phys. Chem. C* **2017**, *121*, 9402–9412.

(15) Cygan, R. T.; Liang, J.-J.; Kalinichev, A. G. Molecular models of hydroxide, oxyhydroxide, and clay phases and the development of a general force field. *J. Phys. Chem. B* **2004**, *108*, 1255–1266.

(16) Rotenberg, B.; Patel, A. J.; Chandler, D. Molecular explanation for why talc surfaces can be both hydrophilic and hydrophobic. *J. Am. Chem. Soc.* **2011**, *133*, 20521–20527.

(17) Marry, V.; Dubois, E.; Malikova, N.; Breu, J.; Haussler, W. Anisotropy of water dynamics in clays: insights from molecular simulations for experimental QENS analysis. *J. Phys. Chem. C* **2013**, *117*, 15106–15115.

(18) Greathouse, J. A.; Hart, D. B.; Bowers, G. M.; Kirkpatrick, R. J.; Cygan, R. T. Molecular simulation of structure and diffusion at smectite-water interfaces: Using expanded clay interlayers as model nanopores. *J. Phys. Chem. C* **2015**, *119*, 17126–17136.

(19) Greathouse, J. A.; Cygan, R. T. Water structure and aqueous uranyl(vi) adsorption equilibria onto external surfaces of beidellite, montmorillonite, and pyrophyllite: results from molecular simulations. *Environ. Sci. Technol.* **2006**, *40*, 3865–3871.

(20) Greathouse, J. A.; Cygan, R. T.; Fredrich, J. T.; Jerauld, G. R. Molecular Dynamics simulation of diffusion and electrical conductivity in montmorillonite Interlayers. *J. Phys. Chem. C* **2016**, *120*, 1640–1649.

(21) Padma Kumar, P.; Kalinichev, A. G.; Kirkpatrick, R. J. Hydration, swelling, interlayer structure, and hydrogen bonding in organolayered double hydroxides: Insights from Molecular Dynamics simulation of citrate-intercalated hydrotalcite. *J. Phys. Chem. B* **2006**, *110*, 3841–3844.

(22) Du, H.; Miller, J. D. A Molecular Dynamics simulation study of water structure and adsorption states at talc surfaces. *Int. J. Miner. Process.* **2007**, *84*, 172–184.

(23) Loganathan, N.; Yazaydin, A. O.; Bowers, G. M.; Kalinichev, A. G.; Kirkpatrick, R. J. Structure, energetics and dynamics of Cs^+ and H_2O in hectorite: Molecular Dynamics simulations with an unconstrained substrate surface. *J. Phys. Chem. C* **2016**, *120*, 10298–10310.

(24) Holmboe, M.; Bourg, I. C. Molecular Dynamics simulations of water and sodium diffusion in smectite interlayer

nanopores as a function of pore size and temperature. *J. Phys. Chem. C* **2014**, *118*, 1001–1013.

(25) Bourg, I. C.; Sposito, G. Connecting the molecular scale to the continuum scale for diffusion processes in smectite-rich porous media. *Environ. Sci. Technol.* **2010**, *44*, 2085–2091.

(26) Zhang, X.; Yi, H.; Zhao, Y.; Min, F.; Song, S. Study on the differences of Na-and Ca-montmorillonites in crystalline swelling regime through Molecular Dynamics simulation. *Adv. Powder Technol.* **2016**, *27*, 779–785.

(27) Tinnacher, R. M.; Holmboe, M.; Tournassat, C.; Bourg, I. C.; Davis, J. A. Ion adsorption and diffusion in smectite: Molecular, pore, and continuum scale views. *Geochim. Cosmochim. Acta* **2016**, *177*, 130–149.

(28) Wang, J.; Kalinichev, A. G.; Kirkpatrick, R. J. Effects of substrate structure and composition on the structure, dynamics, and energetics of water at mineral surfaces: A Molecular Dynamics modeling study. *Geochim. Cosmochim. Acta* **2006**, *70*, 562–582.

(29) Greathouse, J. A.; Cygan, R. T. Molecular Dynamics simulation of uranyl(vi) adsorption equilibria onto an external montmorillonite surface. *Phys. Chem. Chem. Phys.* **2005**, *7*, 3580–3586.

(30) Wang, J.; Kalinichev, A. G.; Kirkpatrick, R. J.; Hou, X. Molecular modeling of the structure and energetics of hydrotalcite hydration. *Chem. Mater.* **2001**, *13*, 145–150.

(31) Kalinichev, A. G.; Kirkpatrick, R. J. Molecular dynamics modeling of chloride binding to the surfaces of calcium hydroxide, hydrated calcium aluminate, and calcium silicate phases. *Chem. Mater.* **2002**, *14*, 3539–3549.

(32) Wang, J.; Kalinichev, A. G.; Kirkpatrick, R. J. Molecular modeling of water structure in nano-pores between brucite (001) surfaces. *Geochim. Cosmochim. Acta* **2004**, *68*, 3351–3365.

(33) Wang, J.; Kalinichev, A. G.; Kirkpatrick, R. J.; Cygan, R. T. Structure, energetics, and dynamics of water adsorbed on the muscovite (001) surface: A Molecular Dynamics simulation. *J. Phys. Chem. B* **2005**, *109*, 15893–15905.

(34) Wang, J.; Kalinichev, A. G.; Kirkpatrick, R. J. Asymmetric hydrogen bonding and orientational ordering of water at hydrophobic and hydrophilic surfaces: A comparison of water/vapor, water/talc, and water/mica interfaces. *J. Phys. Chem. C* **2009**, *113*, 11077–11085.

(35) Kirkpatrick, R. J.; Kalinichev, A. G.; Hou, X.; Struble, L. Experimental and Molecular Dynamics modeling studies of interlayer swelling: water incorporation in kanemite and ASR gel. *Mater. Struct.* **2005**, *38*, 449–458.

(36) Kerisit, S.; Liu, C.; Ilton, E. S. Molecular Dynamics simulations of the orthoclase (001)-and (010)-water interfaces. *Geochim. Cosmochim. Acta* **2008**, *72*, 1481–1497.

(37) Wander, M. C. F.; Clark, A. E. Structural and dielectric properties of quartz-water interfaces. *J. Phys. Chem. C* **2008**, *112*, 19986–19994.

(38) Cygan, R. T.; Greathouse, J. A.; Heinz, H.; Kalinichev, A. G. Molecular models and simulations of layered materials. *J. Mater. Chem.* **2009**, *19*, 2470–2481.

(39) Malani, A.; Ayappa, K. G. Adsorption isotherms of water on mica: Redistribution and film growth. *J. Phys. Chem. B* **2009**, *113*, 1058–1067.

(40) Michot, L. J.; Ferrage, E.; Jiménez-Ruiz, M.; Boehm, M.; Delville, A.

Anisotropic features of water and ion dynamics in synthetic Na- and Ca-smectites with tetrahedral layer charge. A combined quasi-elastic neutron-scattering and Molecular Dynamics simulations study. *J. Phys. Chem. C* **2012**, *116*, 16619–16633.

(41) Jungwirth, P.; Tobias, D. J. Specific ion effects at the air/water interface. *Chem. Rev.* **2006**, *106*, 1259–1281.

(42) Wick, C. D.; Cummings, O. T. Understanding the factors that contribute to ion interfacial behavior. *Chem. Phys. Lett.* **2011**, *513*, 161–166.

(43) Wick, C. D.; Kuo, I.-F. W.; Mundy, C. J.; Dang, L. X. The effect of polarizability for understanding the molecular structure of aqueous interfaces. *J. Chem. Theory Comput.* **2007**, *3*, 2002–2010.

(44) Kamath, G.; Deshmukh, S. A.; Sankaranarayanan, S. K. R. S. Comparison of select polarizable and non-polarizable water models in predicting solvation dynamics of water confined between MgO slabs. *J. Phys.: Condens. Matter* **2013**, *25*, 305003.

(45) Moučka, F.; Zamfir, S.; Bratko, D.; Luzar, A. Molecular polarizability in open ensemble simulations of aqueous nanoconfinements under electric field. *J. Chem. Phys.* **2019**, *150*, 164702.

(46) Daub, C. D.; Cann, N. M.; Bratko, D.; Luzar, A. Electrokinetic flow of an aqueous electrolyte in amorphous silica nanotubes. *Phys. Chem. Chem. Phys.* **2018**, *20*, 27838–27848.

(47) Tazi, S.; Molina, J. J.; Rotenberg, B.; Turq, P.; Vuilleumier, R.; Salanne, M. A transferable ab initio based force field for aqueous ions. *J. Chem. Phys.* **2012**, *136*, 114507.

(48) Tesson, S.; Salanne, M.; Rotenberg, B.; Tazi, S.; Marry, V. Classical polarizable force field for clays: Pyrophyllite and talc. *J. Phys. Chem. C* **2016**, *120*, 3749–3758.

(49) Tesson, S.; Louisfrema, W.; Marry, V. Classical polarizable force field to study dry charged clays and zeolites. *J. Phys. Chem. C* **2017**, *121*, 9833–9846.

(50) Tesson, S.; Louisfrema, W.; Salanne, M.; Boutin, A.; Ferrage, E.; Rotenberg, B.; Marry, V. Classical polarizable force field to study hydrated charged claysand zeolites. *J. Phys. Chem. C* **2018**, *122*, 24690–24704.

(51) Hånde, R.; Ramothe, V.; Tesson, S.; Dazas, B.; Ferrage, E.; Lanson, B.; Salanne, M.; Rotenberg, B.; Marry, V. Classical polarizable force field to study hydrated hectorite: Optimization on DFT calculations and validation against XRD Data. *Minerals* **2018**, *205*.

(52) Tsipursky, S. I.; Drits, V. A. The distribution of octahedral cations in the 2:1 layers of dioctahedral smectites studied by oblique-texture electron diffraction. *Clay Miner.* **1984**, *19*, 177–193.

(53) Brindley, G. W.; Brown, G. *Crystal Structures of Clay Mineralsand their X-Ray Identification*; Mineralogical Society, 1980.

(54) Ferrage, E.; Lanson, B.; Michot, L. J.; Robert, J.-L. Hydration properties and interlayer organization of water and ions in synthetic Na-smectite with tetrahedral layer charge. part 1. Results from X-Ray diffraction profile modeling. *J. Phys. Chem. C* **2010**, *114*, 4515–4526.

(55) Teleman, O.; Jonsson, B.; Engstrom, S. A Molecular Dynamics simulation of a water model with intramolecular degrees of freedom. *Mol. Phys.* **1987**, *60*, 193–203.

(56) Berendsen, H. J. C.; Postma, J. P. M.; van Gunsteren, W. F.; Hermans, J. Interaction models for water in relation to protein hydratation. *The Jerusalem Symposia on Quantum Chemistry and Biochemistry* **1981**, *14*, 331–342.

(57) Berendsen, H. J. C.; Grigera, J. R.; Straatsma, T. P. The missing term in effective pair potentials. *J. Phys. Chem.* **1987**, *91*, 6269–6271.

(58) Guillot, B. A reappraisal of what we have learnt during three decades of computer simulations on water. *J. Mol. Liq.* **2002**, *101*, 219–260.

(59) Laage, D.; Hynes, J. T. A molecular jump mechanism of water reorientation. *Science* **2006**, *311*, 832–835.

(60) Smith, D. E.; Dang, L. X. Computer simulations of NaCl association in polarizable water. *J. Chem. Phys.* **1994**, *100*, 3757–3766.

(61) Dang, L. X.; Chang, T.-M. Molecular Dynamics study of water clusters, liquid, and liquid-vapor interface of water with many-body potentials. *J. Chem. Phys.* **1997**, *106*, 8149–8159.

(62) Masia, M.; Probst, M.; Rey, R. On the performance of molecular polarization methods. I. water and carbon tetrachloride. *J. Chem. Phys.* **2004**, *121*, 7362–7378.

(63) Masia, M.; Probst, M.; Rey, R. On the performance of molecular polarization methods. II. water and carbon tetrachloride close to a cation. *J. Chem. Phys.* **2005**, *123*, 164505.

(64) Tazi, S.; Botan, A.; Salanne, M.; Marry, V.; Turq, P.; Rotenberg, B. Diffusion coefficient and shear viscosity of rigid water models. *J. Phys.: Condens. Matter* **2012**, *24*, 284117.

(65) Plimpton, S. Fast parallel algorithms for short-Range Molecular Dynamics. *J. Comput. Phys.* **1995**, *117*, 1–19.

(66) developers group, C. http://cp2k.berlios.de.

(67) Hockney, R. W.; Eastwood, J. W. *Computer Simulation Using Particles*; Taylor and Francis: New York, NY, USA, 1988.

(68) Ewald, P. Evaluation of optical and electrostatic lattice potentials. *Ann. Phys.* **1921**, *64*, 253–287.

(69) Jones, G.; Christian, S. M. The viscosity of aqueous solutions of electrolytes as a function of the concentration. V. Sodium chloride. *J. Am. Chem. Soc.* **1937**, *59*, 484–486.

(70) Ryckaert, J.-P.; Ciccoti, G.; Berendsen, H. J. C. Numerical integration of the cartesian equations of motion of a system with constraints: Molecular Dynamics of n-alkanes. *J. Comput. Phys.* **1977**, *23*, 327–341.

(71) Liu, P.; Harder, E.; ; Berne, B. J. On the calculation of diffusion coefficients in confined fluids and interfaces with an application to the liquid vapor interface of water. *J. Phys. Chem. B* **2004**, *108*, 6595–6602.

(72) Simonnin, P.; Noetinger, B.; Nieto-Draghi, C.; Marry, V.; Rotenberg, B. Diffusion under confinement: hydrodynamic finite-size effects in simulation. *J. Chem. Theory Comput.* **2017**, *122*, 18484–18492.

(73) Fuller, N. G.; Rowley, R. L. The effect of model internal flexibility upon NEMD simulations of viscosity. *Int. J. Thermophys.* **2000**, *21*, 45–55.

(74) Tournassat, C.; Bourg, I. C.; Holmboe, M.; Sposito, G.; Steefel, C. I. Molecular Dynamics simulations of anion exclusion in clay interlayer nanopores. *Clays Clay Miner.* **2016**, *64*, 374–388.

(75) Tournassat, C.; Gaboreau, S.; Robinet, J.-C.; Bourg, I. C.; Steefel, C. I. Impact of microstructure on anion exclusion in compacted clay media. *The Clay Minerals Society Workshop Lectures Series* **2015**, *21*, 137–149.

(76) Jardat, M.; Dufrêche, J.-F.; Marry, V.; Rotenberg, B.; Turq, P. Salt exclusion in charged porous media: A coarse-graining strategy in the case of montmorillonite

clays. *Phys. Chem. Chem. Phys.* **2009**, *11*, 2023–2033.

(77) Molina, J. J.; Dufrêche, J.-F.; Salanne, M.; Bernard, O.; Turq, P. Primitive models of ions in solution from molecular descriptions: A perturbation approach. *J. Chem. Phys.* **2011**, *135*, 234509.

(78) Krynicki, K.; Green, C. D.; Sawyer, D. W. Pressure and temperature dependence of self-diffusion in water. *Faraday Discuss. Chem. Soc.* **1978**, *66*, 199–208.

(79) Wallqvist, A.; Teleman, O. Properties of flexible water models. *Mol. Phys.* **1991**, *74*, 515–533.

(80) Simonnin, P.; Marry, V.; Noetinger, B.; Nieto-Draghi, C.; Rotenberg, B. Mineral and ion specific effects at clay water interfaces: Structure, diffusion, and hydrodynamics. *J. Phys. Chem. C* **2018**, *122*.

(81) Botan, A.; Marry, V.; Rotenberg, B.; Turq, P.; Noetinger, B. How electrostatics influences hydrodynamic boundary conditions: Poiseuille and electro-osmostic flows in clay nanopores. *J. Phys. Chem. C* **2013**, *117*, 978–985.

(82) Churakov, S. V.; Prasianakis, N. I. Review of the current status and challenges for a holistic process-based description of mass transport and mineral reactivity in porous media. *Am. J. Sci.* **2018**, *318*, 921–948.

(83) Churakov, S. V.; Gimmi, T. Up-scaling of molecular diffusion coefficients in clays: A two-step approach. *J. Phys. Chem. C* **2011**, *115*, 6703–6714.

(84) Borukhov, I.; Andelman, D.; Orland, H. Steric effects in electrolytes: A modified Poisson-Boltzmann equation. *Phys. Rev. Lett.* **1997**, *79*, 435.

(85) Kornyshev, A. A. Double-layer in ionic liquids: Paradigm change? *J. Phys. Chem. B* **2007**, *111*, 5545–5557.

(86) Bhuiyan, L. B.; Outhwaite, C. W.; Henderson, D.; Alawneh, M. A modified Poisson-Boltzmann theory and Monte Carlo simulation study of surface polarization effects in the planar diffuse double layer. *Mol. Phys.* **2007**, *105*, 1395–1402.

(87) Outhwaite, C. W.; Lamperski, S.; Bhuiyan, L. B. Influence of electrode polarization on the capacitance of an electric double layer at and around zero surface charge. *Mol. Phys.* **2011**, *109*, 21–26.

(88) Bohinc, K.; Bossa, G.; May, S. Incorporation of ion and solvent structure into mean-field modeling of the electric double layer. *Adv. Colloid Interface Sci.* **2017**, *249*, 220–233.

(89) Ludl, A.-A.; Bove, L. E.; Corradini, D.; Saitta, A. M.; Salanne, M.; Bull, C. L.; Klotz, S. Probing ice VII crystallization from amorphous NaCl-D_2O solutions at gigapascal pressures. *Phys. Chem. Chem. Phys.* **2017**, *19*, 1875.

(90) Revil, A.; Leroy, P. Constitutive equations for ionic transport in porous shales. *J. Geophys. Res.* **2004**, *109*, B03208.

(91) Liu, L. Prediction of swelling pressures of different types of bentonite in dilute solutions. *Colloids Surf., A* **2013**, *434*, 303–318.

(92) Obliger, A.; Jardat, M.; Coelho, D.; Bekri, S.; Rotenberg, B. Pore network model of electrokinetic transport through charged porous media. *Phys. Rev. E* **2014**, *89*, 043013.

(93) Lipowsky, E.; Sackmann, E. *Structure and Dynamics of Membranes*; Elsevier, 1995.

(94) Carnie, S. L.; Torrie, G. M. *The statistical mechanics of the electrical double layer*; John Wiley & Sons, Inc., 1984.

Graphical TOC Entry